Influence of microfluidic flow rates on the propagation of nano/microcracks in liquid core and hollow fibers

Mohammadreza Naeimirad[a,b,c,*], Ali Zadhoush[c], Rasoul Esmaeely Neisiany[d,e], Seeram Ramakrishna[e], Saeed Salimian[c,f] and A. Andres Leal[b,1]

[a] Department of Materials and Textile Engineering, Faculty of Engineering, Razi University, Kermanshah, Iran

[b] Laboratory for Advanced Fibers, Empa, Swiss Federal Laboratories for Materials Science and Technology, Lerchenfeldstrasse 5, 9014 St. Gallen, Switzerland

[c] Department of Textile Engineering, Isfahan University of Technology, Isfahan 84156-83111, Iran

[d] Department of Chemical Engineering, Isfahan University of Technology, Isfahan 84156-83111, Iran

[e] Center for Nanofibers and Nanotechnology, Department of Mechanical Engineering, Faculty of Engineering, National University of Singapore, Singapore 117576, Singapore

[f] Building Energy Materials & Components, Empa, Swiss Federal Laboratories for Materials Science and Technology, CH-8600 Dübendorf, Switzerland

Corresponding authors e-mail address: m.naeimirad@razi.ac.ir

[1] Present address: Insulation and Polymer Technologies Group, Energy and Materials Department, Corporate Research, ABB Switzerland Ltd., Segelhofstrasse 1K, 5405 Baden, Switzerland.

Abstract

Melt-spinning is a conventional method for the production of synthetic fibers. The development of melt-spun liquid core or liquid filled fibers in which the liquid component is already incorporated during fiber spinning has been reported as a viable alternative to traditional hollow fibers. The elucidation of the mechanical behavior of this new type of bicomponent fiber is of interest, with particular emphasis on its fracture mechanics. In this paper we describe a microfluidics method used to induce liquid flows through these fibers (internal diameter 15 – 30 μm), aiming at analyzing the influence of flow rate on crack formation and/or propagation. Although only a very small number of fibers show the presence of cracks (1 – 4% of the tested specimens), it is possible to establish a clear correlation between flow rate and the appearance of cracks. The main fracture mechanism found to be operating in these melt-spun fibers is the type I (opening mode) fracture, evidenced as the internal pressure exerted by the liquid being injected through the fibers increases during microfluidic testing. As fiber spinning and drawing force the polymer chains that compose the sheath to be preferentially oriented in the fiber direction, the formation of axial cracks over transverse cracks is favored due to a lack of strong intermolecular interactions between polymer chains in the transverse direction of the fiber.

Keywords: Melt-spinning, Liquid core fiber, Fracture, Nano/microcrack, Leakage

Naeimirad, M., Zadhoush, A., Neisiany, R. E., Ramakrishna, S., Salimian, S., & Leal, A. A. (2018). Influence of microfluidic flow rates on the propagation of nano/microcracks in liquid core and hollow fibers. Theoretical and Applied Fracture Mechanics, 96, 83-89. http://doi.org/10.1016/j.tafmec.2018.04.001

1. Introduction

There has always been a high demand for fibrous materials in our society [1]. Besides normal solid cross-sectional fibers, synthetic fibers can be produced in other cross-sections e.g. hollow, delta or even multicomponent configurations [2, 3]. There are three main methods for the production of synthetic staple fibers or continuous filaments from polymeric materials: melt-spinning, wet-spinning and dry-spinning [4, 5]. Multicomponent melt-spinning is a well-established technique for the production of thermoplastic fibers which benefits from the characteristics of two or more different polymers [6]. To produce bicomponent filaments, two molten polymers come together at the outlet of the spinneret to make different configurations such as core/sheath (C/S) or side by side (S/S) [7]. Bicomponent fibers exhibit different properties such as conductivity and self-crimping, based on the configuration and nature of the polymers used in their production [8, 9]. In addition to direct production of hollow fibers through C shape or segmented cross-section spinnerets, dissolving the core part in C/S bicomponent fibers can also provide fibers with perfect circular hollow channels [10]. Hollow fibers are able to provide an optimal performance in numerous applications (e.g. light-weight or thermal isolation), while a growing number of reports in the literature account for the use of hollow filaments and membranes that enable solid-liquid interactions in fields such as microextraction [11].

A popular idea in the fiber science world is to use specific nanomaterials as fillers that impart special properties e.g. antibacterial [12], heat resistance [13], reinforcement [14-17], tribological enhancement [18] and flame retardancy [19]. In a recent work, a liquid core bicomponent fiber (LCF) was produced via continuous high-speed melt-spinning process [20]. For this purpose, different co-flowing morphologies were studied using a transparent co-flowing setup [21] to develop a co-extrusion die [22]. Extrusion trials led to the design of a bicomponent spin pack from which a CFD analysis confirmed that a jetting biphasic flow re-

gime is responsible for the continuous liquid core channel observed in actual experiments [23], enabling the production of such a fiber in a single-step melt-spinning process [20]. The development of such a fine fiber (50 µm in outer diameter) containing a liquid channel (15 µm in diameter) with high-speed winding (1500 m/min) is a promising material for different applications e.g. damping [22], self-healing [24-26], optics [27] and drug delivery [28]. Hufenus et al. [22] reported that the viscose characteristics of the liquid core in LCFs causes higher energy absorption in comparison with conventional synthetic fibers. This novel feature can be exploited by enhancing flexural and fracture resistance in garments, armor, etc. In the same line Leal et al. [28] developed a new technique to manipulate the core liquid in LCFs and inject liquids in hollow and LCFs using a microfluidic approach. They also showed the applicability of the Hagen-Poiseuille theory to analyze the flow of distilled water in both aforementioned fiber types [28]. Meanwhile, microfluidic studies carried out on melt-spun fibers [28] showed the existence of sporadic fluid leakage from the polymeric body, which may be due to the fracture or damage of the sheath during the melt-spinning process, during handling, or as a result of internal pressure induced during microfluidic testing.

Crack formation and propagation are important fracture mechanisms in different materials including polymeric composites and fibers. Fracture and cracks in cylindrical bodies (e.g. fibers or tubular structures) behave differently depending on whether these bodies are composed of brittle or ductile materials. The possible reasons for crack propagation include tensile, flexural and shear stresses as well as fatigue, among others [36]. According to the Irwin's theory there are three classifications corresponding to the crack propagation [37]: mode I, or opening mode, mode II, or sliding mode and mode III, or tearing mode. Moreover, morphological aspects of the polymers such as spherulite nucleation [38], environmental conditions [36], aspect ratio [39], thermal history and residual stresses [40] are very important factors in the formation and propagation of microcracks in cylindrical bodies such as fibers [36] or pipes [41, 42]. Recently, some research has been focused on improving fracture behavior of adhe-

sives [29-32] and developing self-healing materials [33-35] to extend the lifetime of fibrous materials.

Historically, crack analysis on fibers has been a relevant research topic in the field of textile science [36]. Therefore, the purpose of the present work is to study the conditions leading to the leakage of a liquid through the polymer sheath of melt-spun LCF and hollow fibers. For this, a newly developed specimen preparation technique is employed which, in combination with a microfluidics pump, allows to analyze the crack propagation phenomenon. The differences in crack propagation behavior observed for the two fibers under analysis are discussed.

2. Experimental

2.1. Materials

LCFs were produced using polypropylene (PP) as polymeric sheath and complex ester as liquid core, by means of a special spin pack illustrated in a previous paper [28] in combination with a multicomponent melt-spinning pilot plant originally built by Fourné Polymertechnik (Alfter-Impekoven, Germany), also described previously [6]. Hollow fibers with the same outer diameter were produced using a three segmented arcs spinneret from HEH, Germany, with the same PP and processing parameters on the aforementioned melt-spinning pilot plant. More details about melt-spinning process can be found elsewhere [20, 23, 28]. Distilled water was used for the microfluidic experiments and an acidic dye (Bezanyl Red E-3BS 200) was used as a coloring agent to enhance the visibility of the leakages through the microcracks formed on the body of the melt-spun fibers.

2.2. Morphological characterization

Melt-spun LCFs and hollow fibers were subjected to morphological characterization. Fiber cross-sections were analyzed using an optical microscope VHX-100, (Keyence, USA) with magnification of 100-1000X, utilizing normal and polarized light. Longitudinal views of the fibers under analysis were acquired by means of a high-resolution scanning electron microscope (SEM), (S-4800 Hitachi, Japan) with a 2 KV beam. In order to improve the conductivity of the samples during electron microscopy, they were initially coated with a 5 nm layer of gold using a sputter coating machine (Leica ACE-600, Switzerland).

2.3. Specimen preparation

As shown in Figure 1, in order to prepare fiber specimens from melt-spun filaments for microfluidic experiments, a roving composed of 100 filaments is used (a). For this, the folded roving is inserted through a Teflon tube with a diameter of 1 mm (b), allowing a few cm of the roving to stick out from the tube. The exposed fibers are then immersed in two component epoxy (c) and pulled back into the tube (d). Once the epoxy hardens, the tube is cut to obtain a clean cross-section with 200 filaments. The specimen thus prepared serves as an adaptor (e) that allows to connect the fibers to the microfluidics pump (f). With this, the 200 filaments (liquid core or hollow) with lengths of up to 40 cm can be employed as individual microfluidic capillaries.

Figure 1. Steps to prepare microfluidic test specimens from melt-spun filaments

2.4. Microfluidic experiments

Microfluidic tests have been performed using a neMESYS microfluidic syringe pump (Cetony, Germany) with a 14.1 gear that delivers a maximum pusher force of 290 N to four 1 mL/60 mm stroke syringes, allowing to achieve total flow rates in the range of 5–250 µL/min

through 200 filaments. Liquid flow through the fibers was observed with an optical microscope AXIO observer A1 (Zeiss, Germany) equipped with polarized and fluorescent light, allowing to detect the number and extent of the leakages against a white background. A detailed view of the microfluidic setup is illustrated in Figure 2.

Figure 2. A bundle of LCFs during microfluidic testing and its observation under an optical microscope

3. Results and discussion

As reported in our recent papers [20, 23, 28] melt-spinning trials have successfully resulted in production of LCF and hollow fibers in continuous length. Microscopic observations confirmed the cylindrical cross-section for both fibers, as well as the presence of complex ester in LCF [20].

3.1. Morphology

As shown in Figure 3, optical microscopy confirms the preparation of a clean cross-section after slicing the tube containing 200 filaments. Therefore, this method successfully maintains the fibers as open channels for liquid microflow while the gaps between fibers are sealed with the epoxy adhesive. The morphological and mechanical performance of the individual fibers has been studied and reported in a previous contribution [20]. The existence of a continuous, uninterrupted internal channel in the fibers has been confirmed by x-ray microcomputed tomography, as reported elsewhere [28].

Figure 3. Optical micrograph with a zoomed-in region showing the hollow fibers with sealed inter-fiber regions in the Teflon tube

Attachment of the prepared specimens to the syringe pump allowed to carry out microfluidic experimental trials which led to the successful liquid manipulation in LCFs and liquid injection in hollow fibers, as illustrated in Figure 4.

Figure 4. Liquid microflow through melt-spun hollow fibers

As shown in Figure 5 (and Supporting information, Video S1, S2 and S3), in some cases the microfluidic tests led to liquid leakage in a few of the fibers under evaluation, confirming the existence of nano/microcracks on the walls of the fibers.

Figure 5. Leakage from micro-cracks on (a) LCFs and (b) hollow fibers

3.2. Fracture analysis

The results of microfluidic tests for crack analysis on 10 specimens containing 200 LCFs each, and 10 specimens containing 200 hollow fibers each are presented in Table 1 and Table 2 respectively, while

Figure 6 shows the average cumulated number of cracks in LCFs and hollow fibers as a function of microfluidic flow rate (5-200 μL/min).

Table 1. Number of cracks in LCFs microfluidic test, based on the leakages at each flow rate level

Table 2. Number of cracks in hollow fibers microfluidic test, based on the leakages at each flow rate level

First of all, it is important to note that only 1% of the LCFs (wall thickness of 20 μm) and 4.5% of the hollow fibers (wall thickness of 12.5 μm) used in the test presented cracks, high-

lighting the important role played by wall thickness. Interestingly, the results evidence the presence of cracks already at the beginning of the microfluidic test, when operating in the low flow rate range. Also, according to the very low number of leakages recorded at high flow rates, the initiation and propagation of cracks on the fibers' body is either due to damage induced by previous processing steps, or the consequence of weak spots which only require a marginal increase in internal pressure to give way to crack formation and propagation.

Figure 6. Average cumulated number of cracks in 200 (a) hollow fibers and (b) LCFs as a function of microfluidic flow rate

As shown in Table 1 and Table 2, achieving the high flow rates (approximately 200 μL/min) in hollow fibers was simple, due to the fact that the core was initially empty, and the existence of a larger internal diameter (30 μm). In contrast, the presence of the highly viscous oil in the core of the LCFs (contact angle of 30 ^{o} on PP [20]) and their significantly smaller internal diameter (15 μm) caused very high back pressure (BP), making it difficult to pump the colored distilled water through the LCFs.

It is concluded that the hollow fibers suffer more leakages than the LCFs. This is attributed to the higher number of nano/microcracks present in the hollow fibers, which could be created in the spinning, drawing and winding process steps, as well as during handling, since the hollow fiber only has a very thin 12.5 μm polymeric wall, while the LCFs have a wall thickness of 20 μm [20]. Additionally, in the case of the LCFs, the presence of the oil in one hand protects the fibers against bending forces during handling, while on the other hand it enhances the damping properties of the fiber [22]. When liquid is pumped through the fibers during the microfluidic experiments, preferential crack formation at weak spots, coupled with liquid flow through any pre-existing cracks, lead to the appearance of most cracks at relatively low flow rates. At higher flow rates, the cumulated number of cracks reaches a plateau, as observed in Figure 6.

SEM images of damaged fibers are shown in Figure 7 and Figure 8 for crack analysis. In both cases, nano/microcracks were evidenced as the liquid was pumped through the fibers. The main observed fracture mode was type I (opening mode). The pumping of liquid through the fiber leads to an increase of internal pressure which tends to expand the fiber diameter, forcing the cracks to propagate according to a mode I type of fracture: opening mode. It is interesting to see that crack propagation happens in the fiber's axial direction and not in the transverse direction. This is mainly due to the polymer chain parallelization process that takes place during fiber spinning and drawing, which leads to the outstanding axial and poor transverse mechanical properties that fibers are known for. Polypropylene, as most polyolefins, is unable to establish strong lateral interactions (crosslinks or intermolecular hydrogen bonds), providing a preferential path for propagation once a crack is formed [43]. From the SEM micrographs, it was noted that the fiber fracture surfaces were ductile, where extensive plastic flow occurs in the material before fracture. Nevertheless, ductility appeared to decrease with increasing flow rates. Additionally, in the case of the LCF, the osmotic pressure of the oil could eventually play a role in the formation of cracks. Such type of degradation of the matrix has been observed by other researchers in tubular specimens [44].

Figure 7. SEM micrographs of hollow fibers (a) without crack (leakage), (b) cracked segment (c) propagated crack and (d) propagated microcrack at high magnification

Figure 8. SEM images of LCFs (a) before leakage, (b) after leakage and (c) with damaged sheath

Conclusion

Liquid core and hollow fibers were produced using a melt-spinning process. The internal micro channels of the fibers were employed as a new media for microflow, developing a bundling technique and attaching the fiber bundles to a microfluidic pump. The microflow and

leakage behavior of the hollow fibers and LCFs were investigated by means of microfluidic tests and the fracture mechanisms were identified via SEM images of the fractured surfaces. Microfluidic tests indicated that most of the cracks appear in the early stages (low flow rates) of the microfluidic studies. Moreover, LCFs showed a lower number of leakages compared to the hollow fibers. The strengthening and toughening of the LCFs is a result of the thicker sheath walls and the damping properties of the core liquid already present in the fiber. From the SEM images, the main mechanism of crack propagation involves the type I (opening mode) initiated by the mechanical loads during operation in addition to residual stresses, where the cracks are formed preferentially in the axial direction. Optimization of the fiber spinning process can certainly lead to a significant reduction of the already very low proportion of cracks appearing in these fibers. Future work will include a parametric study to analyze the relation between fiber spinning parameters and crack formation, where the insights gained on nano/microcrack formation and propagation will allow to perform an optimization of fiber spinning parameters.

Acknowledgments

The authors would like to thank Benno Wuest and Laura Gottardo for the melt-spinning of the fibers, Josep Puigmarti and Afshin Abrishamkar for their support with the microfluidics experiments, and Prof. Manfred Heuberger and Dr. Rudolf Hufenus for the valuable discussions on this topic.

References

[1] R. Kotek, Recent advances in polymer fibers, Polymer Reviews, 48 (2008) 221-229.

[2] D. Zhang, Advances in filament yarn spinning of textiles and polymers, Elsevier, 2014.

[3] M. Naeimirad, A. Zadhoush, R. Kotek, R. Esmaeely Neisiany, S. Nouri Khorasani, S. Ramakrishna, Recent advances in core/shell bicomponent fibers and nanofibers: A review, Journal of Applied Polymer Science, 135 (2018) 46265.

[4] F. Fourné, Synthetic fibers: machines and equipment, manufacture, properties: handbook for plant engineering, machine design, and operation, Hanser Verlag, 1999.

[5] A. Ziabicki, Fundamentals of Fiber Formation, Wiely Publication, 1974.

[6] R. Hufenus, C. Affolter, M. Camenzind, F.A. Reifler, Design and Characterization of a Bicomponent Melt-Spun Fiber Optimized for Artificial Turf Applications, Macromolecular Materials and Engineering, 298 (2013) 653-663.

[7] S. Houis, F. Schreiber, T. Gries, Fiber Table: Bicomponent fibers (Part 1), Chemical Fibers International, 58 (2008) 38-45.

[8] A. Lund, B. Hagström, Melt spinning of β-phase poly (vinylidene fluoride) yarns with and without a conductive core, Journal of Applied Polymer Science, 120 (2011) 1080-1089.

[9] M. Stråål, M. Rigdahl, B. Hagström, Conducting bicomponent fibers obtained by melt spinning of PA6 and polyolefins containing high amounts of carbonaceous fillers, Journal of Applied Polymer Science, 123 (2012) 936-943.

[10] T. Oh, Studies on melt spinning process of hollow polyethylene terephthalate fibers, Polymer engineering and science, 46 (2006) 609.

[11] Y.-Y. Chao, Z.-X. Jian, Y.-M. Tu, H.-W. Wang, Y.-L. Huang, An on-line push/pull perfusion-based hollow-fiber liquid-phase microextraction system for high-performance liquid chromatographic determination of alkylphenols in water samples, Analyst, 138 (2013) 3271-3279.

[12] S.Y. Yeo, H.J. Lee, S.H. Jeong, Preparation of nanocomposite fibers for permanent antibacterial effect, Journal of Materials Science, 38 (2003) 2143-2147.

[13] S. Salimian, A. Zadhoush, M. Naeimirad, R. Kotek, S. Ramakrishna, A review on aerogel: 3D nanoporous structured fillers in polymer-based nanocomposites, Polymer Composites, http://www.10.1002/pc.24412.

[14] R.E. Neisiany, S.N. Khorasani, M. Naeimirad, J.K.Y. Lee, S. Ramakrishna, Improving Mechanical Properties of Carbon/Epoxy Composite by Incorporating Functionalized Electrospun Polyacrylonitrile Nanofibers, Macromolecular Materials and Engineering, 302 (2017) 1600551.

[15] S. Razavi, R.E. Neisiany, M. Ayatollahi, S. Ramakrishna, S.N. Khorasani, F. Berto, Fracture assessment of polyacrylonitrile nanofiber-reinforced epoxy adhesive, Theoretical and Applied Fracture Mechanics, (2017), https://doi.org/10.1016/j.tafmec.2017.07.023.

[16] A. Zadhoush, R. Reyhani, M. Naeimirad, Evaluation of surface modification impact on PP/MWCNT nanocomposites by rheological and mechanical characterization, assisted with morphological image processing, Polymer Composites, http://www.10.1002/pc.24799.

[17] R.E. Neisiany, S.N. Khorasani, J.K.Y. Lee, M. Naeimirad, S. Ramakrishna, Interfacial toughening of carbon/epoxy composite by incorporating styrene acrylonitrile nanofibers, Theoretical and Applied Fracture Mechanics, 95 (2018) 242-247.

[18] M. Naeimirad, A. Zadhoush, R.E. Neisiany, Fabrication and characterization of silicon carbide/epoxy nanocomposite using silicon carbide nanowhisker and nanoparticle reinforcements, Journal of Composite Materials, 50 (2016) 435-446.

[19] S. Kazemi, M.R.M. Mojtahedi, W. Takarada, T. Kikutani, Morphology and crystallization behavior of nylon 6-clay/neat nylon 6 bicomponent nanocomposite fibers, Journal of Applied Polymer Science, 131 (2014).

[20] M. Naeimirad, A. Zadhoush, A. Abrishamkar, A. Pishevar, A. Leal, Melt-spun liquid core fibers: physical and morphological characteristics, Iranian Polymer Journal, 25 (2016) 397-403.

[21] M. Heuberger, L. Gottardo, M. Dressler, R. Hufenus, Biphasic fluid oscillator with coaxial injection and upstream mass and momentum transfer, Microfluidics and Nanofluidics, (2015) 1-11.

[22] R. Hufenus, L. Gottardo, A.A. Leal, A. Zemp, K. Heutschi, P. Schuetz, V.R. Meyer, M. Heuberger, Melt-spun polymer fibers with liquid core exhibit enhanced mechanical damping, Materials & Design, 110 (2016) 685-692.

[23] M. Naeimirad, A. Zadhoush, Melt-spun liquid core fibers: a CFD analysis on biphasic flow in coaxial spinneret die, Fibers and Polymers, http://www.10.1007/s12221-000-0000-0.

[24] R.E. Neisiany, J.K.Y. Lee, S.N. Khorasani, S. Ramakrishna, Towards the development of self-healing carbon/epoxy composites with improved potential provided by efficient encapsulation of healing agents in core-shell nanofibers, Polymer Testing, 62 (2017) 79-87.

[25] S.N. Khorasani, S. Ataei, R.E. Neisiany, Microencapsulation of a coconut oil-based alkyd resin into poly(melamine–urea–formaldehyde) as shell for self-healing purposes, Progress in Organic Coatings, 111 (2017) 99-106.

[26] F. Safaei, S.N. Khorasani, H. Rahnama, R.E. Neisiany, M.S. Koochaki, Single microcapsules containing epoxy healing agent used for development in the fabrication of cost efficient self-healing epoxy coating, Progress in Organic Coatings, 114 (2018) 40-46.

[27] F. Cox, A. Argyros, M. Large, Liquid-filled hollow core microstructured polymer optical fiber, Optics Express, 14 (2006) 4135-4140.

[28] A.A. Leal, M. Naeimirad, L. Gottardo, P. Schuetz, A. Zadhoush, R. Hufenus, Microfluidic behavior in melt-spun hollow and liquid core fibers, International Journal of Polymeric Materials and Polymeric Biomaterials, 65 (2016) 451-456.

[29] H. Khoramishad, S.M.J. Razavi, Metallic fiber-reinforced adhesively bonded joints, International Journal of Adhesion and Adhesives, 55 (2014) 114-122.

[30] M.R. Ayatollahi, A.N. Giv, S.M.J. Razavi, H. Khoramishad, Mechanical properties of adhesively single lap-bonded joints reinforced with multi-walled carbon nanotubes and silica nanoparticles, The Journal of Adhesion, (2016) 1-18.

[31] S.M.J. Razavi, M.R. Ayatollahi, E. Esmaeili, L.F.M. da Silva, Mixed-mode fracture response of metallic fiber-reinforced epoxy adhesive, European Journal of Mechanics - A/Solids, 65 (2017) 349-359.

[32] S.M.J. Razavi, M.R. Ayatollahi, A. Nemati Giv, H. Khoramishad, Single lap joints bonded with structural adhesives reinforced with a mixture of silica nanoparticles and multi walled carbon nanotubes, International Journal of Adhesion and Adhesives, 80 (2018) 76-86.

[33] R.E. Neisiany, S.N. Khorasani, J. Kong Yoong Lee, S. Ramakrishna, Encapsulation of epoxy and amine curing agent in PAN nanofibers by coaxial electrospinning for self-healing purposes, RSC Advances, 6 (2016) 70056-70063.

[34] R.E. Neisiany, J.K.Y. Lee, S.N. Khorasani, S. Ramakrishna, Self-healing and interfacially toughened carbon fibre-epoxy composites based on electrospun core–shell nanofibres, Journal of Applied Polymer Science, 134 (2017) 44956.

[35] R. Esmaeely Neisiany, J.K.Y. Lee, S. Nouri Khorasani, R. Bagheri, S. Ramakrishna, Facile strategy toward fabrication of highly responsive self-healing carbon/epoxy composites via incorporation of healing agents encapsulated in poly(methylmethacrylate) nanofiber shell, Journal of Industrial and Engineering Chemistry, 59 (2018) 456-466.

[36] J.W. Hearle, B. Lomas, W.D. Cooke, Atlas of fibre fracture and damage to textiles, Elsevier, 1998.

[37] M. Patrıcio, R. Mattheij, Crack propagation analysis, CASA report, (2007) 07-03.

[38] K. Friedrich, Analysis of crack propagation in isotactic polypropylene with different morphology, in: Physik der Duroplaste und anderer Polymerer, Springer, 1978, pp. 103-112.

[39] A. Chudnovsky, A. Moet, R. Bankert, M. Takemori, Effect of damage dissemination on crack propagation in polypropylene, Journal of applied physics, 54 (1983) 5562-5567.

[40] W. Grellmann, S. Seidler, K. Jung, I. Kotter, Crack-resistance behavior of polypropylene copolymers, Journal of applied polymer science, 79 (2001) 2317-2325.

[41] A. Emery, A. Kobayashi, W. Love, B. Place, C. Lee, Y. Chao, An experimental and analytical investigation of axial crack propagation in long pipes, Engineering Fracture Mechanics, 23 (1986) 215-226.

[42] W. Kastner, E. Röhrich, W. Schmitt, R. Steinbuch, Critical crack sizes in ductile piping, International Journal of Pressure Vessels and Piping, 9 (1981) 197-219.

[43] A.A. Leal, O.A. Neururer, A. Bian, A. Gooneie, P. Rupper, K. Masania, C. Dransfeld, R. Hufenus, Inter-facial interactions in bicomponent polymer fibers, Polymer, 142 (2018) 375-386.

[44] G. Moan, C. Coleman, E. Price, D. Rodgers, S. Sagat, Leak-before-break in the pressure tubes of CANDU reactors, International Journal of Pressure Vessels and Piping, 43 (1990) 1-21.

Table Captions

Table 1. Number of cracks in LCFs microfluidic test, based on the leakages at each flow rate level

Table 2. Number of cracks in hollow fibers microfluidic test, based on the leakages at each flow rate level

Figure Captions

Figure 1. Steps to prepare microfluidic test specimens from melt-spun filaments

Figure 2. A bundle of LCFs during microfluidic testing and its observation under an optical microscope

Figure 3. Optical micrograph with a zoomed-in region showing the hollow fibers with sealed inter-fiber regions in the Teflon tube

Figure 4. Liquid microflow through melt-spun hollow fibers

Figure 5. Leakage from micro-cracks on (a) LCFs and (b) hollow fibers

Figure 6. Average cumulated number of cracks in 200 (a) hollow fibers and (b) LCFs as a function of microfluidic flow rate

Figure 7. SEM micrographs of hollow fibers (a) without crack (leakage), (b) cracked segment (c) propagated crack and (d) propagated microcrack at high magnification

Figure *8*. SEM images of LCFs (a) before leakage, (b) after leakage and (c) with damaged sheath

Table 1. Number of cracks in LCFs microfluidic test, based on the leakages at each flow rate level

Specimen No /Flow rate	5 (µL/min)	10 (µL/min)	20 (µL/min)	40 (µL/min)	50 (µL/min)	75 (µL/min)	100 (µL/min)	More
1	1/200	1/199	1/198	2/197	0/195	0/195	BP [1]	-
2	1/200	2/199	0/197	1/197	0/196	0/196	1/196	BP
3	0/200	1/200	0/199	1/199	0/198	BP	-	-
4	1/200	1/199	0/198	0/198	BP	-	-	-
5	1/200	1/199	0/198	BP	-	-	-	-
6	0/200	1/200	BP	-	-	-	-	-
7	0/200	0/200	0/200	BP	-	-	-	-
8	0/200	1/200	0/199	BP	-	-	-	-
9	1/200	0/199	BP	-	-	-	-	-
10	0/200	1/200	1/199	0/198	BP	-	-	-

[1] Back Pressure

Table 2. Number of cracks in hollow fibers microfluidic test, based on the leakages at each flow rate level

Specimen No /Flow rate	5 (µL/min)	10 (µL/min)	20 (µL/min)	50 (µL/min)	100 (µL/min)	150 (µL/min)	200 (µL/min)	More
1	2/200	3/198	4/195	1/191	0/190	0/190	BP	-
2	3/200	1/197	2/196	2/194	1/192	-	BP	-
3	3/200	1/197	1/196	2/195	2/193	1/191	0/190	BP
4	1/200	1/199	1/198	2/197	2/195	-	0/193	BP
5	1/200	1/199	0/198	1/198	1/197	-	BP	-
6	0/200	1/200	2/199	7/197	3/190	0/187	BP	-
7	1/200	1/199	1/198	3/197	2/194	BP	-	-
8	1/200	2/199	0/197	1/197	2/196	2/194	0/192	BP
9	0/200	1/200	3/199	2/196	2/194	0/192	BP	-
10	1/200	1/199	1/198	5/197	4/192	2/188	0/186	BP

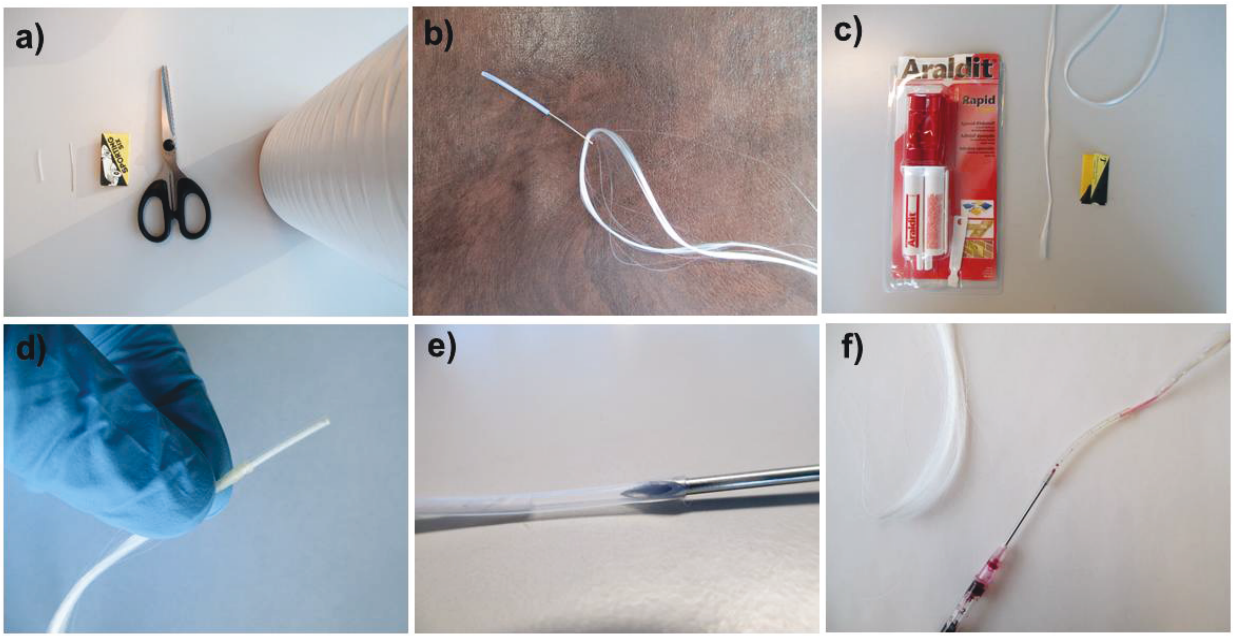

Figure 1. Steps to prepare microfluidic test specimens from melt-spun filaments

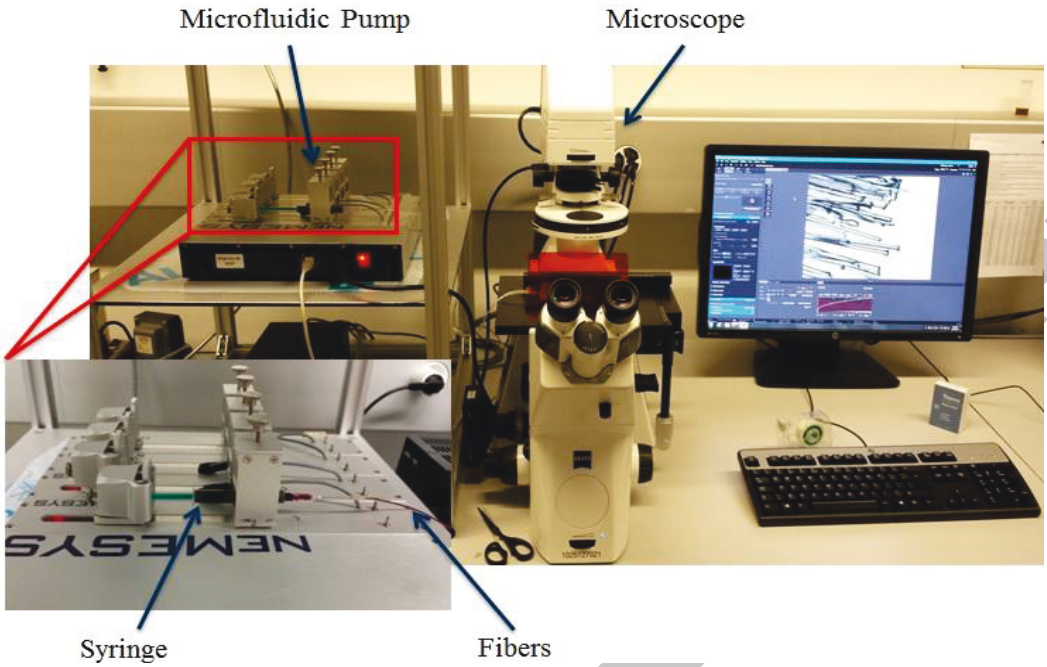

Figure 2. A bundle of LCFs during microfluidic testing and its observation under an optical microscope

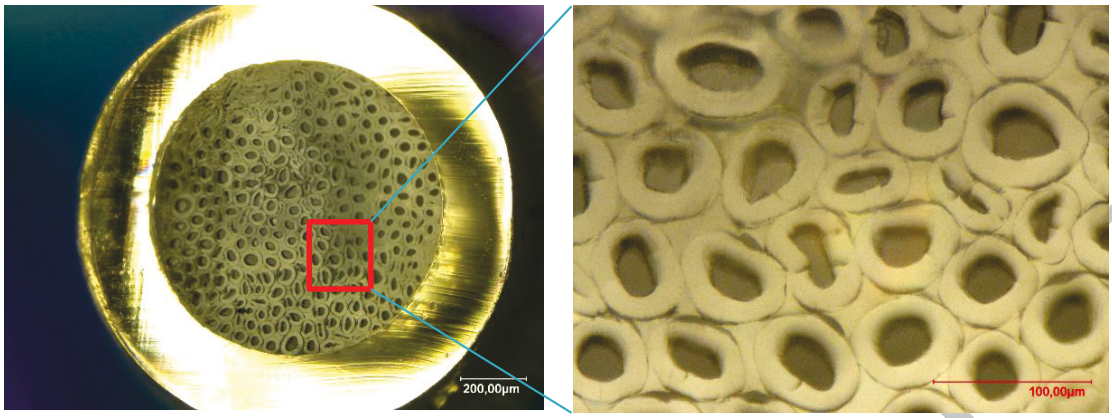

Figure 3. Optical micrograph with a zoomed-in region showing the hollow fibers with sealed inter-fiber regions in the Teflon tube

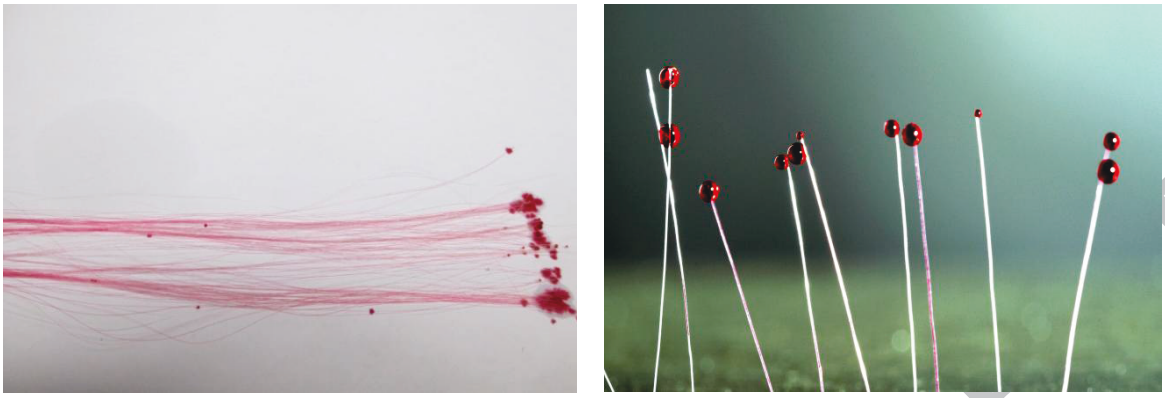

Figure 4. Liquid microflow through melt-spun hollow fibers

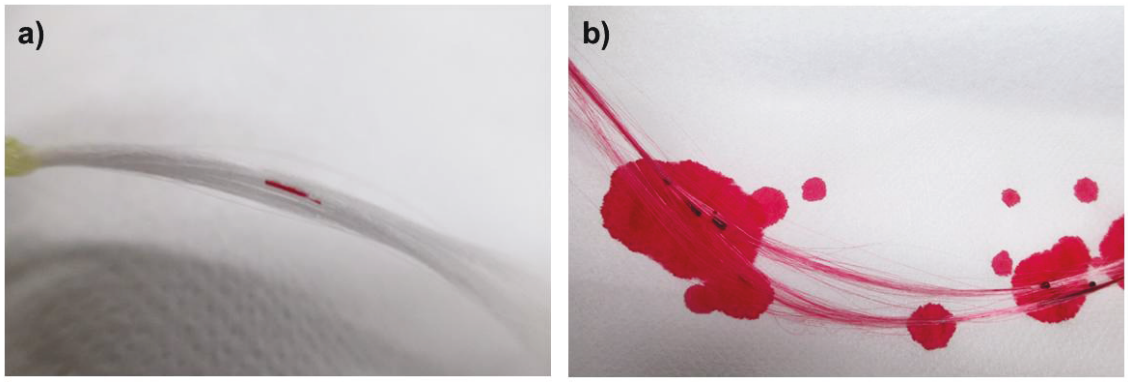

Figure 5. Leakage from micro-cracks on (a) LCFs and (b) hollow fibers

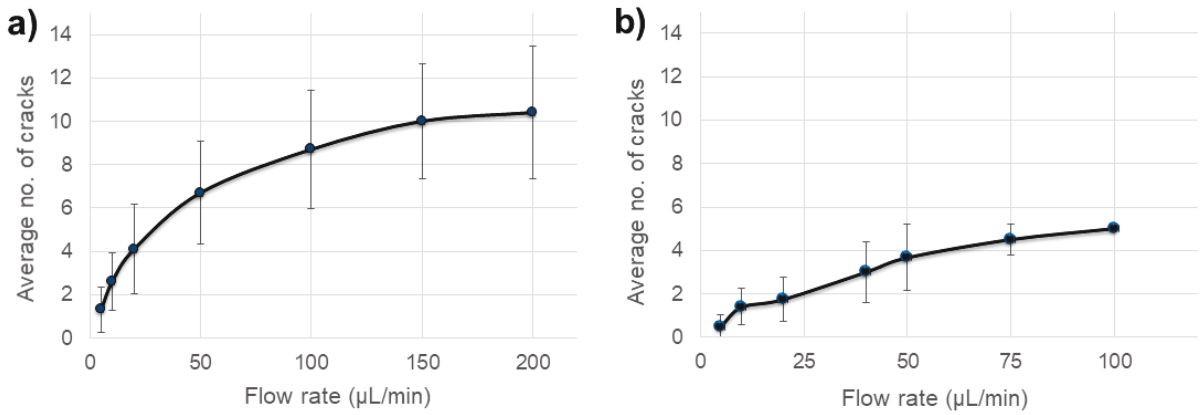

Figure 6. Average cumulated number of cracks in 200 (a) hollow fibers and (b) LCFs as a function of microfluidic flow rate

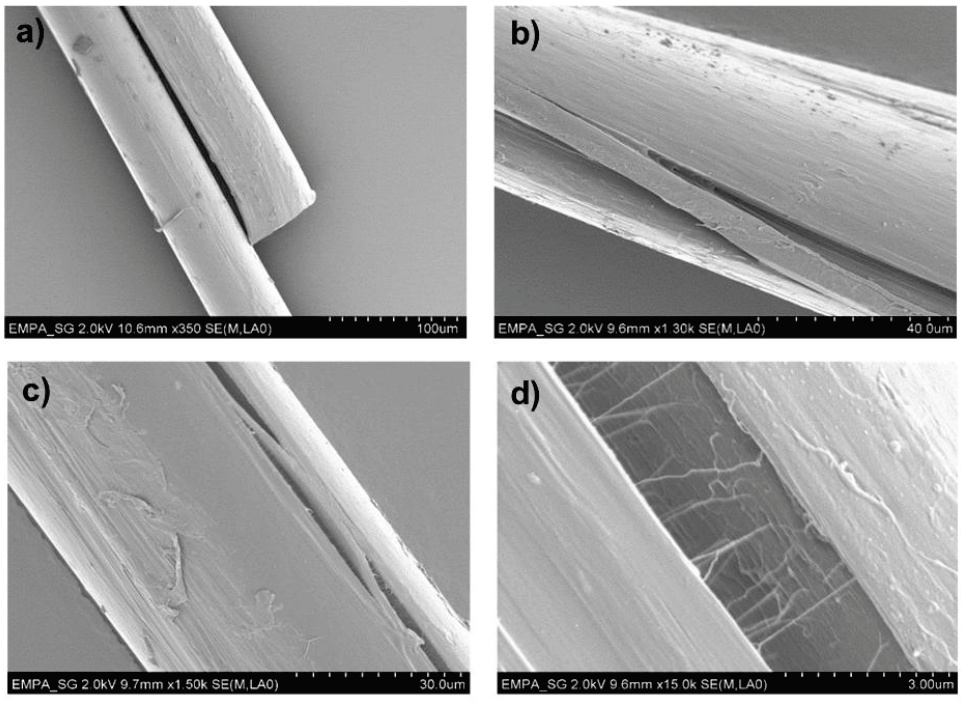

Figure 7. SEM micrographs of hollow fibers (a) without crack (leakage), (b) cracked segment (c) propagated crack and (d) propagated microcrack at high magnification

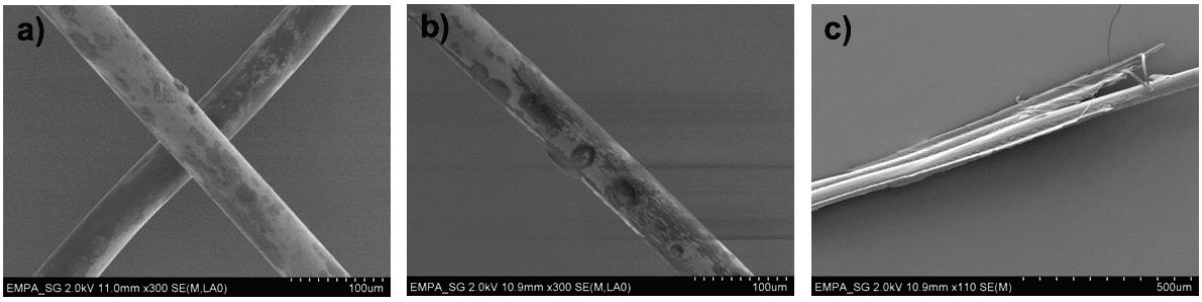

Figure 8. SEM images of LCFs (a) before leakage, (b) after leakage and (c) with damaged sheath

Highlights:

- Liquid core and hollow fibers were spun from polypropylene and complex ester using multicomponent high-speed melt-spinning pilot plant.
- A new technique was developed for bundling melt-spun filaments and attaching to the microfluidic pump.
- Nano/microcrack-induced leakages during the microfluidic trials were used for crack analysis on fine polymeric fibers.
- Liquid core fibers showed less nano/microcracks compare to the hollow fibers.

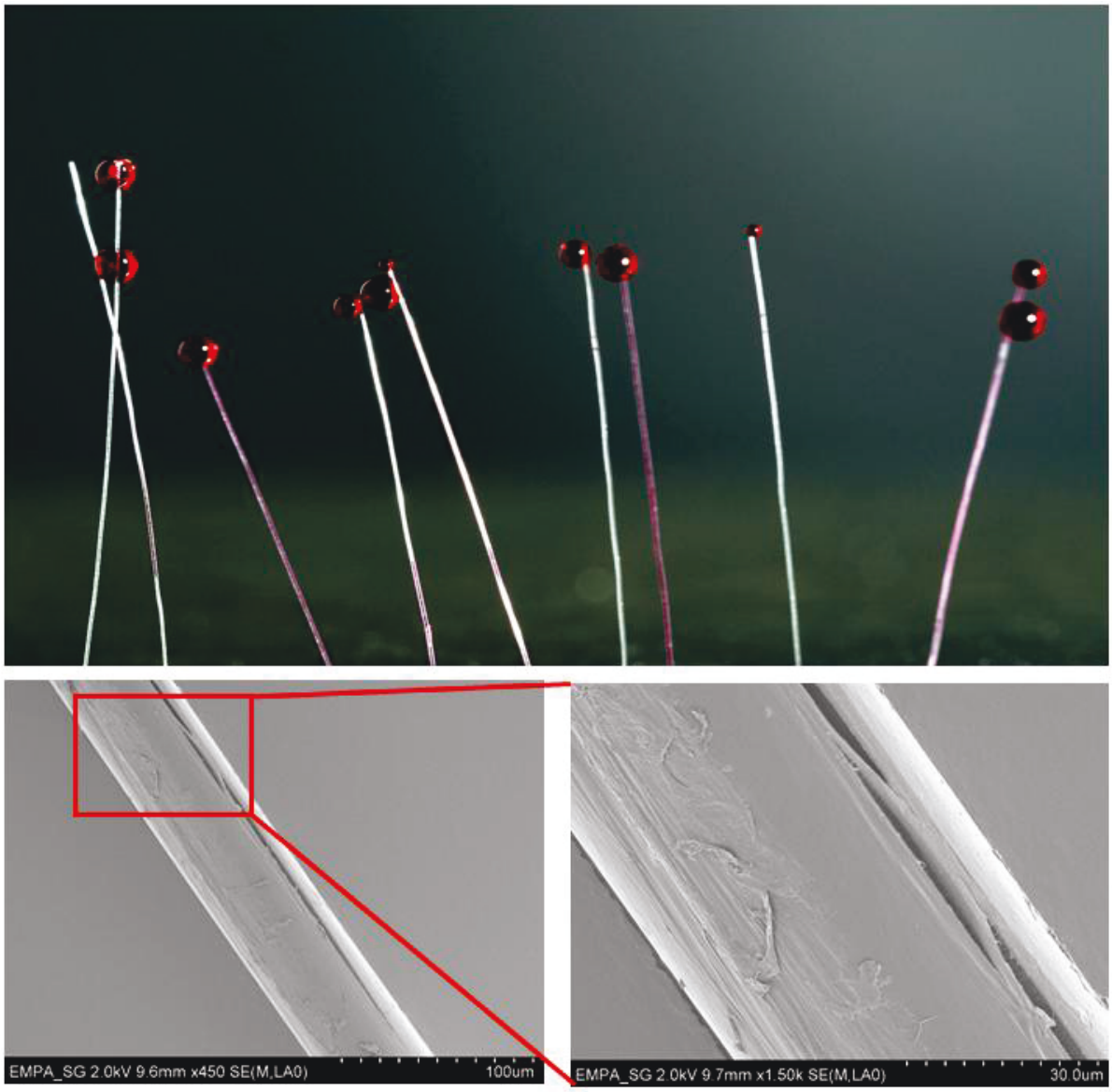
EMPA_SG 2.0kV 9.6mm x450 SE(M,LA0)
100um
EMPA_SG 2.0kV 9.7mm x1.50k SE(M,LA0)
30.0um